Available online at www.sciencedirect.com
ScienceDirect
Journal of Molecular Catalysis A: Chemical 275 (2007) 158–166
JOURNAL OF MOLECULAR CATALYSIS A: CHEMICAL
www.elsevier.com/locate/molcata

Alkylation of benzene and other aromatics by benzyl chloride over iron-containing aluminophosphate molecular sieves

H. Hentit [a], K. Bachari [b,*], M.S. Ouali [a], M. Womes [c], B. Benaichouba [a], J.C. Jumas [c]

[a] *Laboratoire de Valorisation des Matériaux, Université Ibn Badis, BP 227, Mostaganem 27000, Algeria*
[b] *Centre de Recherche Scientifique et Technique en Analyses Physico-Chimiques (C.R.A.P.C.), BP 248, Alger RP 16004, Algiers, Algeria*
[c] *Laboratoire des Agrégats, Interfaces, Matériaux pour l'Energie (AIME) Institut Charles Gerhardt, UMR 5253 CNRS-UMII-ENSCM, Université Montpellier II, CC 15, Place E. Bataillon, 34095 Montpellier Cedex 5, France*

Received 24 April 2007; received in revised form 19 May 2007; accepted 21 May 2007
Available online 25 May 2007

Abstract

Iron-containing aluminophosphate molecular sieves were synthesized in AEL and AFI structure types by static hydrothermal crystallization. These materials have been characterized by elemental analysis, X-ray diffraction, scanning electron microscopy, N_2 adsorption–desorption, temperature programmed desorption of ammonia (NH_3-TPD), and ^{57}Fe Mössbauer spectroscopy. Alkylation of benzene and other aromatics by benzyl chloride has been investigated over these solids. Indeed, the iron containing microporous aluminophosphates showed both high activity and high selectivity for this reaction. The activity of these catalysts for the benzylation of different aromatic compounds is in the following order: benzene > toluene > *p*-xylene > anisole. More interesting is the observation that this catalyst can be reused in the benzylation of benzene for several times. Kinetics of the benzene benzylation over these catalysts has also been investigated.

Keywords: Microporous aluminophosphates; FAPO-5; FAPO-11; Friedel-Crafts alkylation; Benzylation of aromatic compounds; Diphenylmethane

1. Introduction

Friedel-Crafts alkylations are a very important class of reactions commonly used in organic chemistry [1,2]. Among these reactions, the liquid phase benzylation of benzene and other aromatic compounds by benzyl chloride or benzyl alcohol is important for the production of diphenylmethane and substituted diphenylmethane which are industrially important compounds used as pharmaceutical intermediates [3] or fine chemicals [4,5]. These reactions are traditionally catalyzed by Lewis acids in liquid phase using $AlCl_3$, $FeCl_3$, BF_3, $ZnCl_2$ and H_2SO_4 [1,2,5]. However, these acid catalysts are toxic and corrosive. Moreover, the isolation of the product is very difficult and causes severe pollution. The new environmental legislations urge for the replacement of all liquid acids by solid acid catalysts which are environmentally more friendly and allow to minimise pollution and waste [6,7]. Indeed, several solid acid catalysts having a good efficiency have been proposed for the benzylation of benzene and other aromatic compounds. For example, we can cite Ga and Fe-modified ZSM-5 and H-β zeolites [8,9], Fe_2O_3 or $FeCl_3$ deposited on micro [9], meso [9,10] and macroporous materials [9,11], Fe and Sn containing mesoporous molecular sieve materials [12,13], $InCl_3$, $GaCl_3$, $FeCl_3$ and $ZnCl_2$ supported on clays and Si-MCM41 [14], ion-exchanged clays [15], Gallium-containing mesoporous silicas HMS [16], $FeCl_3$, $MnCl_2$, $NiCl_2$ and $ZnCl_2$ supported on acidic alumina [17]. Zeolites such as H-ZSM-5 and H-β have been shown to be effective for alkylation of several aromatic compounds such as phenols or naphtols [18,19]. However, poor results have been obtained for the benzylation of benzene over the previously mentioned catalysts [20]. Choudhary et al. [9,21] reported that the activity of ZSM-5 and H-β zeolites increases when other phases (Ga, Al or Fe; as metal oxides or chlorides) are added to the zeolites framework. Among these elements, iron has been observed to be the additive that improves the catalysts performance to the highest extent.

Microporous like-zeolite aluminophosphates (AlPOs) molecular sieves have attracted much interest since the first

* Corresponding author.
E-mail address: bachari2000@yahoo.fr (K. Bachari).

1381-1169/$ – see front matter © 2007 Elsevier B.V. All rights reserved.
doi:10.1016/j.molcata.2007.05.032

synthesis by Wilson in 1982 [22] due to their catalytic and sorptive properties [23–28]. The structure of AlPOs consists of a combination of aluminium and phosphate ions where trivalent aluminium and tetravalent phosphorous are in tetrahedral environment in the dehydrated material [29]. In the field of catalysis, the incorporation of various elements in the AlPO framework leads to the synthesis of new materials with novel acidic or redox properties [30–33].

Several studies concerning the iron incorporated aluminophosphate molecular sieves have been reported [34–38]. Beside the shape selectivity of the aluminophosphate framework, it has been shown that the incorporation of iron into these materials modifies the acidity of AlPOs solids and creates isolated redox centres by isomorphous lattice substitution. Thus, potential applications as catalysts for hydrocarbon conversion and oxidation combustion reaction over the FAPOs catalysts have been investigated [33,39,40]. However, studies of the benzylation of aromatics over these materials have not been reported in our knowledge.

In the present work, the possibility of the isomorphous substitution of iron into an $AlPO_4$-5 (AFI) and $AlPO_4$-11 (AEL) matrix has been studied using different physico-chemical methods. Furthermore, an investigation has been undertaken to study the synthesised Fe containing amluminophosphates for their performances as catalysts in the benzylation of benzene and other aromatics by benzyl chloride and to propose a mechanism for this reaction.

2. Experimental

2.1. Catalysts synthesis

$AlPO_4$-5, $AlPO_4$-11, $FAPO_4$-5 and $FAPO_4$-11 were synthesised hydrothermally according to the literature [22,34,41] The aluminium and phosphorous sources were aluminium isopropoxyde (Fluka) and phosphoric acid (85%, Prolabo), respectively. Iron(III) chloride hexahydrate (Prolabo) was used as the iron source. The templating agents were triethylamine (98%, Fluka) for $AlPO_4$-5 and $FAPO_4$-5 and di-*n*-propylamine (98%, Fluka) for $AlPO_4$-11 and $FAPO_4$-11. The gel compositions and the synthesis conditions are given in Table 1. The starting mixtures were heated in a Teflon-lined autoclave for crystallization. At the end of the heat treatment the autoclave was quenched in water. The solid products were filtered, washed with distilled water and air dried, first at room temperature overnight, then at 353 K for 8 h. Calcination of the molecular sieves has been performed in air at 823 K for 6 h to remove the organic template.

2.2. Catalysts characterization

X-ray diffraction (XRD) patterns were recorded on a Philips X'PERT Diffractometer using Cu Kα radiation and nickel filters. Measures were recorded with 0.02° (2θ) per step and 1 s counting time per step. An inductively coupled plasma atomic emission spectrometer (ICP-AES, Varian model Liberty (II) axial view) was used for chemical analysis of the samples. Scanning electron microscopy (SEM) was performed on a FEI Quanta200 and analyses of the samples were conducted in an attached X-rays microanalyzer. BET surface area measurements, using nitrogen at 77 K, were carried out on micrometrics ASAP2010 equipment. All the samples have been outgased overnight at 493 K before the analysis. The isotherms were used to calculate the BET specific surface area, total pore volume and average pore diameter according to the Horvath–Kawazoe method. Temperature programmed desorption (TPD) of NH_3 was carried out on micrometrics Autochem 2910 equipment. All samples were first activated at 823 K (5 K/min) for 120 min under helium (20 ml/min). Ammonia (30 ml/min) was injected at 373 K to saturate the sample. Measurements of desorbed ammonia were performed from 373 to 823 K. Iron doped materials were characterised by ^{57}Fe Mössbauer spectroscopy at room temperature on a standard EG and G constant acceleration spectrometer in transmission mode using ^{57}Co*Rh* as the γ-ray source. The velocity scale was calibrated using the magnetic sextuplet spectrum of a high purity iron foil absorber and the origin of isomer shift scale was determined from the centre of the α-Fe spectrum. Fe hyperfine parameters were determined by fitting Lorentzian lines to the experimental data using the ISO fit programme [42].

2.3. Catalytic reaction

The benzylation reactions over a series of iron-containing microporous aluminophosphates catalysts were carried out in a magnetically stirred glass reactor (25 cm^3) fitted with a reflux condenser, having a low dead volume, mercury thermometer and arrangement for continuously bubbling moisture free nitrogen N_2 (flow rate = 30 cm^3/min) through the liquid reaction mixture, at the following reaction conditions: reaction mixture = 15 ml of moisture-free liquid aromatic compound (or 2.5 ml of moisture-free aromatic compound mixes with 12.5 ml of moisture-free solvent) + 1.0 ml of benzyl chloride, amount of

Table 1
Gel composition and preparation conditions of the materials

Sample	Synthesis gel ratios (mole)					PH	Pretreatment		Crystallization	
	Al_2O_3	P_2O_5	Fe_2O_3	R	H_2O		Temperature (K)	Time (h)	Temperature (K)	Time (h)
$AlPO_4$-5	1	1	0	1.4	70	7.53	–	–	473	24
$AlPO_4$-11	1	1	0	1.4	70	7.39	–	–	473	40
$FAPO_4$-5	0.9	1	0.1	1.4	70	10.26	263	96	473	24
$FAPO_4$-11	0.9	1	0.1	1.4	70	9.54	263	96	473	40

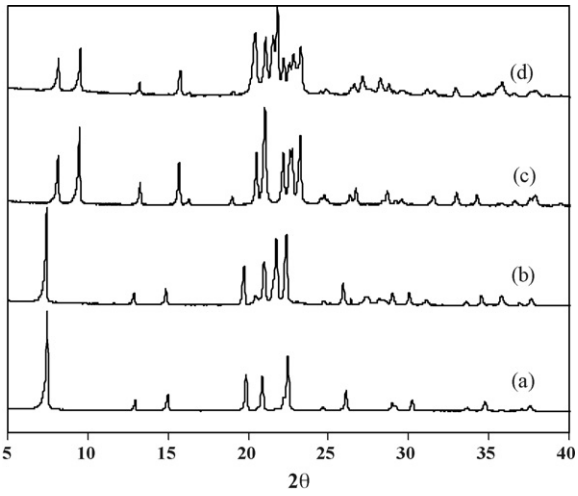

Fig. 1. XRD patterns of as-synthesized (a) $AlPO_4$-5, (b) $FAPO_4$-5, (c) $AlPO_4$-11 and (d) $FAPO_4$-11.

catalyst = 0.1 g and reaction temperature = 353 K. The reaction was started by injecting benzyl chloride in the reaction mixture, containing catalyst and aromatic compound with or without solvent. Measuring quantitatively the HCl evolved in the reaction by acid–base titration (by absorbing the HCl carried by N_2 in a 0.1 M NaOH solution containing phenolphthalein indicator) followed the course of the reaction. The polybenzyl chloride (which is formed by the condensation of benzyl chloride) was isolated from the reaction mixture by the procedure given by Choudhary et al. [9]. In all the cases, the major product formed was mainly mono-benzylated compound along with polybenzyl chloride as side product depending upon the condition used. Samples were analyzed periodically on a gas chromatograph (HP-6890) equipped with a FID detector and a capillary column RTX-1 (30 m × 0.32 nm i.d.).

3. Results and discussion

3.1. Characterization

The XRD patterns of as-synthesised materials are shown in Fig. 1. The high crystallinity of the obtained material is clearly illustrated. For AlPO-5 and AlPO-11 X-ray diffractograms are identical to those presented in the literature characterising AFI and AEL crystalline phases, respectively [22]. The synthesised $FAPO_4$-5 and $FAPO_4$-11 solids were identified to be principally AFI and AEL phases, respectively, with a minor proportion of an unidentified crystalline composition. We can see from the XRD patterns that the incorporation of iron in the AFI and AEL framework changes drastically the cell parameters. This is reflected by a shift of peaks in the 2θ region between 19° and 24° for $FAPO_4$-5 as compared to $AlPO_4$-5. The peak at 19.8° corresponding to the (2 1 0) reflection is shifted to 20.4° and the peaks at around 22.4°, corresponding to the (1 0 2) and (2 1 1) reflections, appear at 21.6° and 21.8°, respectively. For $FAPO_4$-11, notable shifts are observed on practically all peaks in the 2θ region between 21.5° and 23.3°. These changes in XRD patterns bear some relation with the size, shape and morphology of the crystals. However, further research is needed to arrive at more precise conclusions.

The scanning electron micrographs of the obtained solids are shown in Fig. 2. The micrographs show that the solids appear as polycrystalline aggregates and the incorporation of iron into the aluminophosphate structure affects the size and the shape of the crystals. The hexagonal morphology of $AlPO_4$-5 is clearly illustrated and hexagonal prisms with 16.5 μm height and 11.5 μm thickness are obtained (Fig. 2a). The incorporation of iron into the AFI structure leads to a hexagonal plate-like morphology (Fig. 2b) and we can notice a crystalline growth along the *c*-axis. The $AlPO_4$-11 crystals are formed from elongated prisms aggregated into spheres (Fig. 2c) and $FAPO_4$-11 crystals have an elongated lamellar morphology (Fig. 2d). Elemental analysis was performed on several single crystals and the averaged results are presented in Table 2 assuming the error of the standard deviation of this analysis. The obtained results allow us to deduce that the incorporation of iron in the aluminophosphate framework is inhomogeneous and iron may occupy aluminium sites. On the other hand, the iron content of the synthesized aluminophosphate is lower than that of the initial gel. Thus, $FAPO_4$ samples can be synthesised only within a very narrow range of iron concentrations. BET surface areas, pores volumes and average pore diameters of the obtained solids are presented in Table 3. The BET surface area values are typical of microporous materials. We can notice that the insertion of iron into the aluminophosphate framework leads to a decrease of the BET surface area and pore volume which can be explained by a change of the pore shape due to the change of the cell parameters. NH_3-TPD was used in order to characterize the acidity of the synthesised aluminophosphates. The results are presented in Fig. 3. The peak at about 420 K found for all samples is due to the desorption of ammonia. The comparison of the TPD curves lets conclude on an increase of the acidity when iron is incorporated in the AlPOs structures (Table 3).

Table 2
Elemental analysis of the catalysts

	$FAPO_4$-5			$FAPO_4$-11		
	Al	P	Fe	Al	P	Fe
Average composition	46 ± 3	48 ± 4	6.0 ± 0.5	45 ± 4	49 ± 4	6.0 ± 0.5
Single crystal	47 ± 4	50 ± 4	3.0 ± 0.2	48 ± 4	49 ± 4	3.0 ± 0.2
Aggregate crystals	37 ± 3	50 ± 4	13 ± 1	42 ± 4	49 ± 4	9.0 ± 0.7
Bulk chemical analysis (normalized atom%)	37.2	57.3	5.5	41.5	52.9	5.6

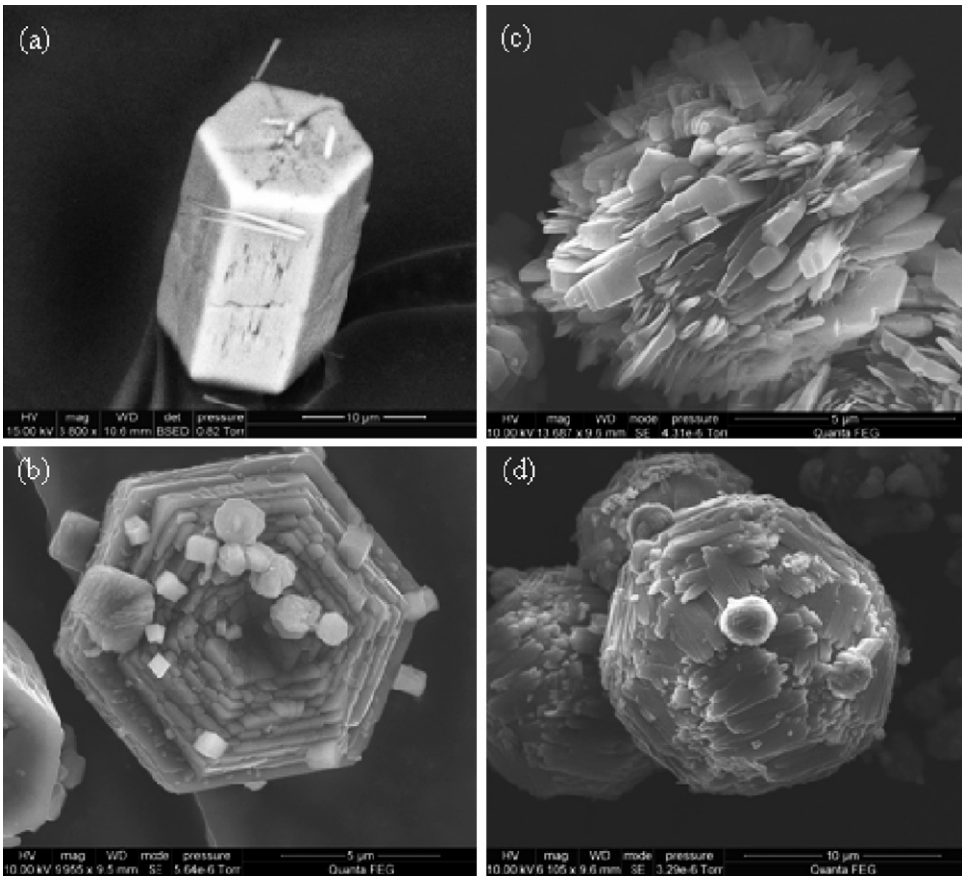

Fig. 2. Scanning electron micrographs of (a) $AlPO_4$-5, (b) $FAPO_4$-5, (c) $AlPO_4$-11 and (d) $FAPO_4$-11.

Table 3
Textural characteristics and acidity of the catalysts

Sample	BET surface area (m^2/g)	Pore volume (cm^3/g)	Average pore diameter (Å)	Desorbed NH_3 (mmol/g)
$AlPO_4$-5	198.59	0.072	5.6	0.095
$AlPO_4$-11	130.40	0.039	6.4	0.253
$FAPO_4$-5	92.02	0.035	5.3	0.301
$FAPO_4$-11	90.48	0.030	6.2	0.255

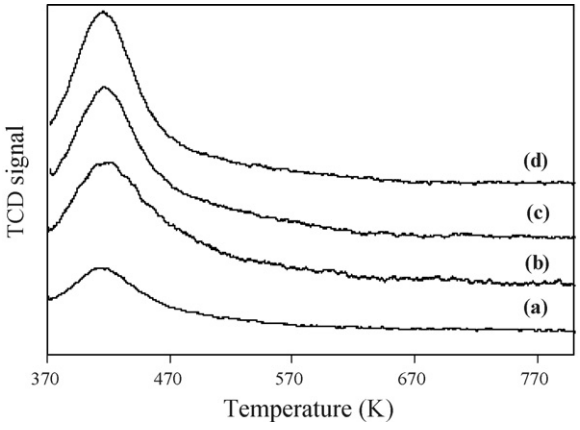

Fig. 3. Temperature programmed desorption of ammonia over (a) $AlPO_4$-5, (b) $FAPO_4$-5, (c) $AlPO_4$-11 and (d) $FAPO_4$-11.

^{57}Fe Mössbauer measurements were performed on as-synthesised and calcined iron containing aluminophosphates in order to obtain more precise information about the nature of the iron species in the crystals. The resulting spectra at room temperature are presented in Fig. 4 and the hyperfine parameters obtained from the corresponding fits (isomer shift (δ), quadrupole splitting (Δ), peak linewidth (Γ) and relative peak areas (A)) are collected in Table 4. The Mössbauer spectra of as-synthesised $FAPO_4$-5 and $FAPO_4$-11 are characterized by a rather broad doublet at $\delta \cong 0.4$ mm/s corresponding to a Fe^{3+} species and several less intense doublets at $\delta = 0.95 \ldots 1.17$ mm/s corresponding to Fe^{2+} species. Thus, some reduction of Fe^{3+} by the structure-templating amine takes place during sample preparation [34]. This reduction is more important in the presence of triethylamine, where the relative peak areas of all Fe^{2+} species amount to 34%, than with di-*n*-propylamine where they represent 6%. Mössbauer spectra of as-synthesised $FAPO_4$-

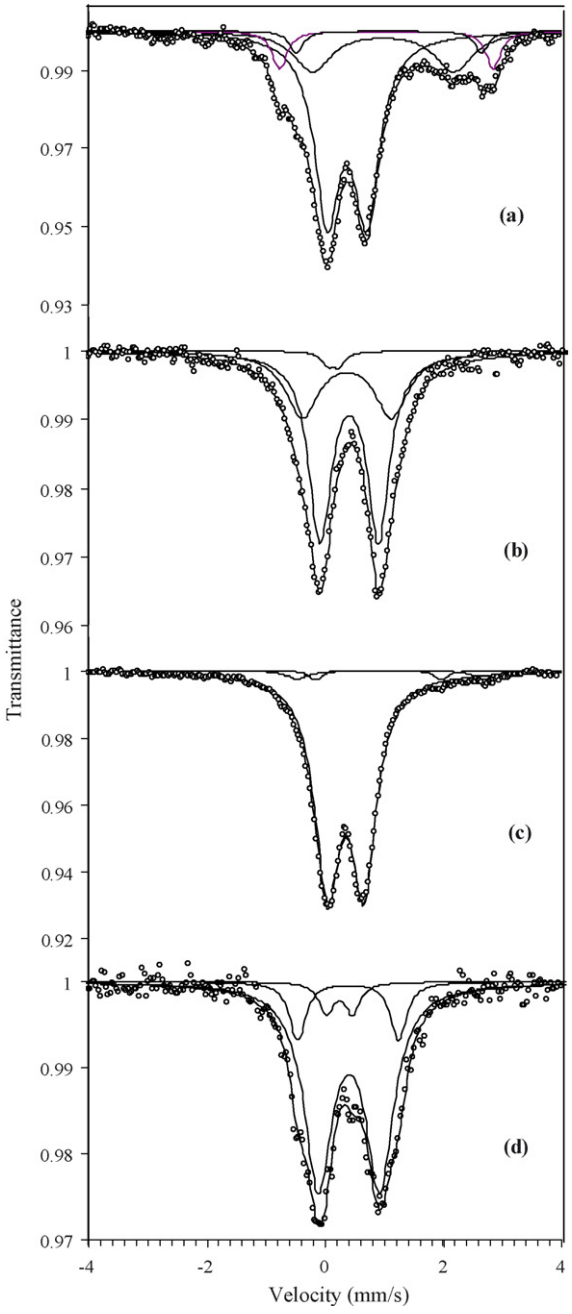

Fig. 4. Mössbauer spectra at room temperature of (a) as-synthesised FAPO-5, (b) calcined FAPO-5, (c) as-synthesised FAPO-11, (c) calcined FAPO-11.

5 fit four doublets showing four different phases. One doublet ($\delta = 0.41$ mm/s) is assigned to octahedral Fe^{3+} [34,38]. Two doublets with isomer shifts of 1.08 and 1.13 mm/s are assigned to octahedral Fe^{2+} [38]. The isomer shift of the fourth doublet, $\delta = 1.03$ mm/s, lies at the lower limit of the values usually found for iron in six-fold oxygen coordination [43]. The important linewidth of 0.72 mm/s lets us conclude that this doublet describes a distribution of various different iron sites comprising octahedral as well as tetrahedral coordinations. The Mössbauer spectrum of $FAPO_4$-11 consists of three doublets, of which one with an isomer shift of 0.39 mm/s is assigned to octahedral Fe^{3+}, while the two others with $\delta = 0.9$ and 1.05 mm/s are characteristic of tetrahedral and octahedral Fe^{2+}, respectively. From this data concerning as-synthesised FAPOs samples, it is evident that all the majority of iron is octahedrally coordinated. On the other hand, chemical analysis indicates that the iron ions may be incorporated in the lattice occupying the aluminium positions. Octahedral symmetry in such sites can be achieved only if the Fe ions are located on the inner pore surface where they have the possibility to interact with molecules trapped in the pores, which can be template or water molecules [38].

In the calcined FAPO-5 and FAPO-11 materials, the divalent Fe species seemed to be oxidized to Fe^{3+} for the two materials. The tetrahedrally coordinated Fe^{3+} species are characterised by isomer shift values of 0.13 mm/s for FAPO-5 and 0.14 for FAPO-11 and low quadrupole splitting values. These species are assumed to substitute for aluminium [38]. Two octahedral Fe^{3+} species are obtained for the two materials, with high values of quadrupole splitting indicating the high distortion of the octahedral symmetry. According to the literature [37,38], this species may be attributed to octahedral Fe^{3+} ions present in lattice defect sites which are coordinated both to bridging lattice oxygen and to terminal oxygen atoms created by bond rupture and ligand coordination. However, presence of extraframework Fe^{3+} species cannot be excluded.

It is worth noting that the Fe^{3+} doublets of all samples are characterised by an important linewidth, each representing iron in a variety of environments differing somewhat by their local symmetry rather than iron on a well-defined crystallographic site. It can further be noted that the calcination increases the average quadrupole splitting of octahedral Fe^{3+}, reflecting changes of the local symmetry induced by the decomposition of template and water molecules.

3.2. Catalytic performances of the synthesized materials

The $AlPO_4$-5, $FAPO_4$-5, $AlPO_4$-11 and $FAPO_4$-11 are compared for their performance in the benzene benzylation reaction in excess of benzene (stochiometric ratio Bz/BzCl = 15) at 353 K. The results are given in Table 5. Comparing these results, we can notice that $AlPO_4$-5 and $AlPO_4$-11 show no catalytic activity for this reaction and that the $FAPO_4$-5 catalyst gives the highest conversion rate with the best selectivity in the benzylation reaction.

3.3. Reaction kinetics

The kinetic data for the benzylation of benzyl reaction in excess of benzene can be fitted into a pseudo-first order rate law [12]:

$$\log\left[\frac{1}{1-x}\right] = \left(\frac{k_a}{2.303}\right)(t - t_0)$$

where k_a is the apparent first-order rate constant, x the fractional conversion of benzyl chloride, t the reaction time and t_0 the induction period corresponding to the time required for reaching equilibrium temperature. A plot of $\log[1/(1-x)]$ as a function of the time gives a linear plot over a large range of benzyl chloride conversions [12].

Table 4
Mössbauer parameters of as-synthesized and calcined iron containing aluminophosphates at room temperature

Samples	δ (mm/s)	Δ (mm/s)	2Γ (mm/s)	A (%)	Attribution	χ^2
As-synthesized $FAPO_4$-5	0.41(1)	0.68(1)	0.53(1)	66	Octahedral Fe^{3+}	0.589
	1.03(3)	2.42(5)	0.78(7)	22	Tetrahedral/octahedral Fe^{2+}	
	1.08(2)	3.65(3)	0.30(4)	8	Octahedral Fe^{2+}	0.411
	1.13(2)	3.17(4)	0.28(8)	4	Octahedral Fe^{2+}	
Calcined $FAPO_4$-5	0.39(1)	0.98(1)	0.46(2)	64	Octahedral Fe^{3+}	
	0.35(4)	1.51(7)	0.68(4)	33	Octahedral Fe^{3+}	
	0.13(4)	0.18(4)	0.24(10)	3	Tetrahedral Fe^{3+}	
As-synthesized $FAPO_4$-11	0.39(1)	0.62(1)	0.51(1)	94	Octahedral Fe^{3+}	1.229
	0.95(3)	2.15(4)	0.31(6)	2	Tetrahedral Fe^{2+}	
	1.17(4)	3.20(6)	0.51(9)	4	Tetrahedral Fe^{2+}	
Calcined $FAPO_4$-11	0.42(2)	0.94(3)	0.52(3)	67	Octahedral Fe^{3+}	0.416
	0.39(4)	1.63(4)	0.44(5)	27	Octahedral Fe^{3+}	
	0.14(2)	0.63(3)	0.23(5)	6	Tetrahedral Fe^{3+}	

(δ) Isomer shift, (Δ) quadrupole splitting, (Γ) peak linewidth, (A) relative peak areas.

Table 5
Catalytic properties of the catalysts in the benzylation of benzene by benzyl chloride at 353k, Bz/BzCl ratio = 15 and m_{cat} = 0.1 g

Materials	Time[a] (min)	Selectivity (%)		Apparent rate constant, k_a ($\times 10^3$ min^{-1})
		Diphenyle methane	Polybenzyl chloride	
AlPO-5	–[b]	–	–	–
AlPO-11	–[b]	–	–	–
$FAPO_4$-5	85.9	98.8	1.2	69.5
$FAPO_4$-11	103.4	95.6	4.4	55.2

[a] Time required for 90% conversion of benzyl chloride.
[b] No reactivity of the material.

Table 6
Influence of the reaction temperature in the benzylation of benzene over $FAPO_4$-5 catalyst (Bz/BzCl ratio = 15, m_{cat} = 0.1 g)

Temperature (K)	Time[a] (min)	Selectivity (%)		Apparent rate constant, k_a ($\times 10^3$ min^{-1})
		Diphenyl methane	Polybenzyl chloride	
343	96.9	100.0	–	51.1
348	91.4	99.5	0.5	60.3
353	85.9	98.8	1.2	69.5

[a] Time required for 90% conversion of benzyl chloride.

The effect of temperature on the rate was studied by conducting the reaction, over the $FAPO_4$-5 catalyst, at 343, 348 and 353 K under the standard reaction's conditions (Bz/BzCl = 15, 0.1 g catalyst). The results show that the catalytic performances of $FAPO_4$-5 increase with the reaction temperature (Table 6). The time necessary for 90% conversion of benzyl chloride and the apparent rate constant k_a changed from 96.9 min and 51.1×10^{-3} min^{-1} at 343 K to 85.9 min and 69.5×10^{-3} min^{-1} at 353 K, respectively, and interestingly, no significant changes of the selectivity occur. The activation energy estimated from the Arrhenius plot is 31 kJ mol^{-1} (Fig. 5)

Table 7 shows the influence of different substituent groups attached to aromatic benzene nucleus on the conversion of benzyl chloride in the benzylation of corresponding substituted benzene over the $FAPO_4$-5 catalyst (0.1 g of catalyst at 353 K) are presented in Table 7. According to the classical

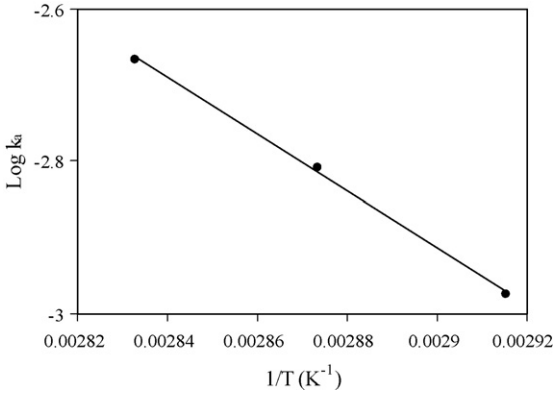

Fig. 5. Arrhenius plot of log k_a as a function of (1/T) for the benzene benzylation reaction over $FAPO_4$-5 catalyst.

Table 7
Reaction rate for benzylation of substituted benzene over $FAPO_4$-5catalyst at 353 K, $m_{cat} = 0.1$ and substituted Bz/BzCl ratio = 15

Substituent	R	σ^+	E_s	k_a ($\times 10^3$ min^{-1})
Benzene	H	0	0	69.5
Toluene	CH_3	−0.31	−1.24	59.3
p-Xylene	$2CH_3$	−0.62	−2.48	47.7
Anisole	OCH_3	−0.78	−0.55	33.4

mechanism of the Friedel-Crafts type acid catalyzed benzylation reaction, the benzylation of an aromatic compound will be easier if one or more donating groups are present in the aromatic ring [1]. In this case, a correlation of the Hammett type would be expected, i.e. $\log k_a = \log k_{a0} + \sigma^+\rho$, where k_{a0} is the rate constant for benzene, σ^+ a coefficient representing the changes of reactivity due to the substituent and ρ is a constant related to the charge on the intermediate complex [44]. Surprisingly, in the present case, the activity of the $FAPO_4$-5 catalyst for the benzylation of the aromatic compounds with donating groups is opposite to that expected from the classical mechanism (Table 7). Thus, the first-order rate constant for the benzylation of benzene and substituted benzenes is in the following order: benzene > toluene > *p*-xylene > anisole. This indicates that, for this catalyst, the reaction mechanism is different from that for the classical acid catalyzed benzylation reactions. Fig. 6 shows a linear relation between the ionization potential of the substrates [45] and $\log k_a$ indicating that the rate constant is more directly related to the ionization potential rather than to σ^+. As indicated earlier, the high activity of the Fe containing catalysts in the benzene benzylation is controlled mostly by their redox property ($Fe^{3+} + e^- \rightarrow Fe^{2+}$). A redox mechanism for the benzylation over Fe containing aluminophosphate in the AFI and AEL structure type can thus be suggested as follows:

$$C_6H_5CH_2{-}Cl + Fe^{3+} \rightarrow C_6H_5CH_2{-}Cl^{\bullet+} + Fe^{2+} \quad (1)$$

$$C_6H_5CH_2{-}Cl^{\bullet+} \rightarrow C_6H_5CH_2^{+} + Cl^{\bullet} \quad (2)$$

$$Fe^{2+} + Cl^{\bullet} \rightarrow Fe^{3+} + Cl^{-} \quad (3)$$

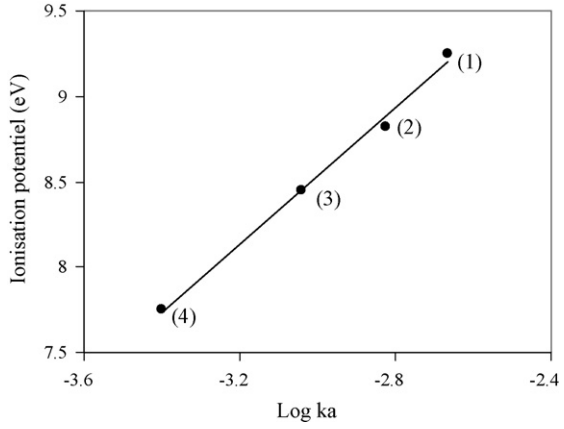

Fig. 6. Log k_a for the benzene benzylation reaction over $FAPO_4$-5 catalyst as a function of the ionization potential tabulated for the different substrates [44]. (1) Benzene, (2) toluene, (3) *p*-xylene, (4) anisole.

Table 8
catalytic activity of $FAPO_4$-5 catalyst for different Bz/BzCl ratios at 353 K ($m_{cat} = 0.1$ g)

Benzene/benzyl chloride ratio	Time[a] (min)	Selectivity (%)	
		Diphenyl methane	Polybenzyl chloride
5	92.7	78.2	21.8
15	85.9	98.8	1.2

[a] Time required for 90% conversion of benzyl chloride.

$$C_6H_5CH_2^{+} + Ar{-}H \rightarrow C_6H_5{-}CH_2{-}Ar + H^{+} \quad (4)$$

$$H^{+} + Cl^{-} \rightarrow HCl \quad (5)$$

Indeed, the formation of reactive species from the benzyl chloride by homolytic rupture of the carbon-chloride bound should be the determining step for the reaction. This mechanism was first proposed to rationalise the catalytic properties of exchanged clays [15] and then generalised for benzene benzylation [10,12,21] and alkylation or acetylation reactions [46] over several iron containing microporous or mesoporous catalysts.

The Taft relation [44] was applied to study the influence of steric effects on the reaction rate. According to this relation, when the steric effect influences the reaction, there is a linear relation between the rate and the parameter E_s which is considered to be representative of the size of the substituting group of the studied aromatic compounds. Using E_s parameters tabulated by Charton [47], it follows from our results in Table 7 that no such relation exists in the case of the benzylation of studied aromatic compounds over the $FAPO_4$-5 catalyst.

3.4. Influence of the stochiometric ratio Bz/BzCl

Two Bz/BzCl ratios were investigated. The obtained results are reported in Table 8. It appears that the stochiometric ratio between benzene and benzyl chloride has a strong influence on the selectivity towards diphenyl methane. Low values of this ratio favour secondary reactions to dibenzylbenzenes and tribenzylbenzenes, eventually because the surface concentration of the reactive molecules derived from benzyl chloride might be too high, favouring in this way the formation of products with more than two rings.

3.5. Influence of the solvent

The role of the solvent in the benzylation of benzene with benzyl chloride was investigated carrying out the reaction with two different solvents: dichloroethane and *n*-heptane. The reaction conditions and the results of benzene benzylation with the $FAPO_4$-5 catalyst are presented in Table 9. The reaction rate is highest in the absence of any solvent. It slightly decreases in dichloroethane, while the decrease in *n*-heptane is more pronounced. The observed dependence of the reaction rate on the solvent is expected because of the competing adsorption of both the reactants and the solvent on the catalyst and because of the high solubility of the polymer in dichloroethane and its weak solubility in *n*-heptane. Indeed, when the polymer solubility in a particular solvent is low, then the polybenzyl formed on

Table 9
effect of the solvent on the conversion of benzyl chloride over $FAPO_4$-5 catalyst (Bz/BzCl ratio = 15, m_{cat} = 0.1 g)

Solvent	Time[a] (min)	Apparent rate constant, k_a ($\times 10^3$ min^{-1})
Without solvent	85.9	69.5
Dichloroethane	87.0	64.9
n-Heptane	88.7	62.6

[a] Time required for 90% conversion of benzyl chloride.

Table 10
Effect of recycling of the catalysts in the benzylation of benzene with benzyl chloride at 353 K over $FAPO_4$-5 catalyst, Bz/BzCl ratio = 15 and m_{cat} = 0.1 g

Catalyst	Time[a] (min)	Selectivity (%)		Apparent rate constant, k_a ($\times 10^3$ min^{-1})
		Diphenyl methane	Polybenzyl chloride	
Fresh	85.4	98.8	1.2	69.5
First reuse	86.0	97.2	2.8	66.8
Second reuse	86.8	95.6	4.4	65.3

[a] Time required for 90% conversion of benzyl chloride.

the catalyst surface is not removed from it which can lead to its deactivation due to the occupation of its active sites by the product formed during the initial reaction. The results show that between these two solvents dichloroethane is a better choice for the benzylation reaction.

3.6. Recycling of the catalysts

The stability of the catalysts was studied by running the benzylation reaction successively with the same catalyst ($FAPO_4$-5) under the same conditions without any regeneration between two runs. The reaction was first run under the standard conditions (benzene to benzyl chloride ratio of 15, 353 K) to the complete conversion of benzyl chloride. Then, after a period of 10 min, benzyl chloride was added to the reaction mixture in such an amount that the initial benzene to benzyl chloride ratio of 15 was established again. After the completion of the second run, the same protocol was repeated a second time. The results, presented in Table 10, show that the catalyst can be used several times in the benzene benzylation process without a significant change of its catalytic activity and selectivity.

4. Conclusion

In the present work, iron-containing aluminophosphate materials of the AFI and AEL structure types were synthesised hydrothermally. Structural characterizations allow us to notice that incorporation of iron into the aluminophosphate has an important effect on the cell parameters and the crystalline morphology. On the other hand, chemical analysis indicates that the majority of Fe ions substitute for Al. Mössbauer spectroscopy reveals that during the synthesis procedure a part of Fe^{3+} is reduced to Fe^{2+} by the templating amines. In as-synthesised and calcined samples, the majority of iron ions is octahedrally coordinated and is assumed to be located on the inner pore surface, in defect sites or in interaction framework sites. Existence of iron on extra-framework species is not excluded.

The study of the benzylation of benzene and other aromatics with benzyl chloride using the synthesised microporous aluminophosphate leads to the following conclusions:

- The microporous AlPO-5 and AlPO-11 alone in the absence of iron species are not active.
- Comparison of the iron-containing aluminophosphate catalysts shows that FAPO-5 gives higher conversion rates than FAPO-11.
- The reaction mechanism involves a redox step at the reaction initiation. This gives a greater independence against the influence of substituents, and FAPOs catalysts can therefore be used with substrates of low reactivity.
- The benzene benzylation is influenced by the solvent used in the process. Among dichloroethane and *n*-heptane, the former is a better solvent for the reaction.
- FAPOs catalysts can be easily reused many times without significant changes in their catalytic performances.

References

[1] G.A. Olah, Friedel-Crafts and Related Reactions, Wiley-Interscience, New York, 1963.
[2] G.A. Olah, Friedel-Crafts Chemistry, Wiley, New York, 1973.
[3] T.W. Bastock, J.H. Clark, Speciality Chemicals, Elsevier, London, 1991.
[4] B.M. Khadilkar, S.D. Borkar, Chem. Technol. Biotechnol. 71 (1998) 209.
[5] R. Commandeur, N. Berger, P. Jay, J. Kervennal, Eur. Pat. Appl. EP 0442 986 (1991) to Atochem S.A.
[6] J.H. Clark, S.R. Cullen, S.J. Barlow, T.W. Bastock, J. Chem. Soc. Perkin Trans. (1994) 1117.
[7] J. Cao, N. He, C. Li, J. Dong, Q. Xu, Mesopor. Mol. Sieves 117 (1998) 461.
[8] V.R. Choudhary, S.K. Jana, N.S. Patil, S.K. Bhargava, Micropor. Mesopor. Mater. 57 (2003) 21.
[9] V.R. Choudhary, S.K. Jana, A.S. Mamman, Micropor. Mesopor. Mater. 56 (2002) 65.
[10] K. Bachari, O. Cherifi, J. Mol. Catal. 260 (2006) 19.
[11] S.G. Pai, A.R. Bajpai, A.B. Deshpande, S.D. Samant, Synth. Commun. 27 (1997) 2267.
[12] K. Bachari, J.M.M. Millet, B. Benaichouba, O. Cherifi, F. Figueras, J. Catal. 221 (2004) 55.
[13] K. Bachari, O. Cherifi, Appl. Catal. A: Gen. 319 (2007) 259.
[14] V.R. Choudhary, S.K. Jana, J. Mol. Catal. A: Chem. 180 (2002) 267.
[15] T. Cseri, S. Bekassy, S. Rizner, F. Figueras, J. Mol. Catal.: A 98 (1995) 101.
[16] K. Bachari, O. Cherifi, J. Mol. Catal. 253 (2006) 187.
[17] M. Salavati-Niasari, J. Hasanalian, H. Najafian, J. Mol. Catal. A 209 (2004) 209.
[18] S.R. Kirumakki, N. Nagaraju, K.V.R. Chary, S. Narayanan, J. Catal. 221 (2004) 549.
[19] A.J. Hoefnagel, H. van Bekkum, Catal. Lett. 85 (2003) 7.
[20] V.C. Chaube, Catal. Commun. 5 (2004) 321.
[21] V.R. Choudhary, S.K. Jana, Appl. Catal. A 224 (2002) 51.
[22] S.T. Wilson, B.M. Lok, E.M. Flanigen, US Patent 4,310,440 (1982).
[23] B. Rajesh, M. Palanichamy, V. Kazansky, V. Murugesan, J. Mol. Catal. A 187 (2002) 259.
[24] H.O. Pastore, S. Coluccia, L. Marchese, Annu. Rev. Mater. Res. 35 (2005) 351.
[25] D.B. Akolekar, Appl. Catal. A: Gen. 171 (1998) 261.
[26] S.H. Jhung, H.K. Kim, J.W. Yoon, J.S. Chang, J. Phys. Chem. B 110 (2006) 9371.

[27] T. Muňoz, K.J. Balkus, Chem. Mater. 10 (1998) 4114.
[28] R. Roque-Malherbe, Micropor. Mesopor. Mater. 41 (2000) 227.
[29] F. Cora, C.R.A. Catlow, J. Phys. Chem. B 105 (2001) 10278.
[30] M. Hartmann, Chem. Rev. 99 (1999) 635.
[31] H. Nur, H. Hamdan, Mater. Res. Bull. 36 (2001) 315.
[32] G. Lischke, B. Parlitz, U. Lohse, E. Schreier, R. Fricke, Appl. Catal. A: Gen. 166 (1908) 351.
[33] E.P.S. Dai, R.H. Petty, C.W. Ingram, R. Szostak, Appl. Catal. A: Gen. 143 (1996) 101.
[34] C.M. Cardile, N.J. Tap, N.B. Milstone, Zeolites 10 (1990) 90.
[35] J.W. Park, H. Chon, J. Catal. 133 (1992) 159.
[36] J. Das, V.V. Satyanaryana, D.K. Chakrabarty, S.N. Piramanayagam, S.N. Shringi, J. Chem. Soc. Faraday Trans. 88 (1992) 3255.
[37] G. Catana, J. Pelgrims, R.A. Schoonheydt, Zeolites 15 (1995) 475.
[38] A. Bruckner, U. Lohse, H. Mehner, Micropor. Mesopor. Mater. 20 (1998) 207.
[39] M.J. Fan, B. Li, R. Cao, J. Catal. Lett. 37 (1994) 189.
[40] P. Tian, Z. Liu, Z. Wu, L. Xu, Y. He, Catal. Today 93–95 (2004) 735.
[41] C.A. Messina, B.M. Lok, E.M. Flanigen, U.S. Patent 4,554,143 (1985).
[42] W. Kündig, Nucl. Instrum. Methods 75 (1969) 336.
[43] F. Menil, J. Phys. Chem. Solids 46 (1985) 763.
[44] J. March, Advanced Organic Chemistry, third ed., Wiley/Interscience, New York, 1985.
[45] D.R. Lide, Handbook of Chemistry and Physics, CRC Press, Boca Raton, FL, 1992.
[46] K. Biro, S. Bekassy, B. Agai, F. Figueras, J. Mol. Catal. A: Chem. 151 (2000) 179.
[47] B. Charton, J. Am. Chem. Soc. 97 (1975) 1552.